

# Characterization of Nb Interface Segregation During Welding Thermal Cycle in Microalloyed Steel by Atom Probe Tomography



H.H. WANG, J. WANG, Z. TONG, P.D. HODGSON, X.L. WAN, K.M. WU, R. WEI,  
and I. TIMOKHINA

Coarse-grained, welding heat-affected zone microstructure was simulated in a Nb-bearing microalloyed steel. The granular bainite with a great number of martensite-austenite (M-A) constituents was the predominant phase. Using atom probe tomography (APT), the distributions of niobium at prior austenite grain boundary (PAGB), ferrite/martensite-austenite (M-A) constituent interface (FMAI), and ferrite/ferrite interface (FFI) were investigated. The binding energy of Nb atom and vacancy was predicted to be 0.45 eV, indicating that Nb segregation by welding thermal cycle is probably a result of the nonequilibrium mechanism. The maximum enrichment of Nb was found at FMAI with enrichment factor of 3.50. Intermediate enrichment of Nb was at PAGB with enrichment factor of 3.12. The interfacial excess of Nb solute element  $\Gamma^{\text{Nb}}$  at PAGB determined by APT was  $0.27 \times 10^{19}$  atoms/m<sup>2</sup>. The segregation energy was calculated to be 22.91 kJ/mol. The minimum enrichment of Nb was at FFI with an enrichment factor of 1.80.

<https://doi.org/10.1007/s11661-018-4940-5>

© The Minerals, Metals & Materials Society and ASM International 2018

## I. INTRODUCTION

WELDING of niobium-bearing microalloyed steels was described as “Myths and Magic”<sup>[1]</sup> due to many disagreements and some controversy on the role of niobium on the impact toughness of welding heat-affected zone (HAZ) in these steels.<sup>[2]</sup> Some researchers revealed that the small addition of Nb (0.01 to 0.04 wt pct) deteriorated the impact toughness of HAZ.<sup>[3–5]</sup> On the contrary, other researchers have demonstrated that Nb had beneficial effects or no significant influence on impact toughness, depending on the carbon level in the high-strength low-alloy (HSLA) steels and welding heat input.<sup>[6–10]</sup> It has been reported<sup>[11–13]</sup> that a small amount of Nb in the solid solution can lower  $\gamma \rightarrow \alpha$  transformation temperature leading to the formation of non-polygonal ferrite microstructure and increase in the yield strength. This effect has generally been attributed to the segregation of Nb to the prior austenite grain

boundaries.<sup>[14,15]</sup> Moreover, Nb was found to promote the formation of martensite-austenite constituent (M-A), which decreased the absorbed energy.<sup>[11,13]</sup> Recent research has indicated that an addition of more than 0.10 wt pct Nb in the pipeline steel led to excellent impact toughness of HAZ even with higher welding heat input.<sup>[16]</sup> This was attributed to the grain refinement.<sup>[16]</sup> Our previous study has suggested that the addition 0.10 wt pct Nb promoted the bainite transformation, and increased the temperature of bainite transformation to ~ 700 °C, which is higher than the conventional bainite transformation temperature. Furthermore, over a large range of cooling rate, bainite was the predominant transformation product in HSLA steel after continuous cooling.<sup>[17]</sup> The formation of bainite within a wide range of cooling rates can potentially increase the volume fraction of the stable, retained austenite that, in turn, improves toughness.<sup>[17,18]</sup>

It was confirmed<sup>[19,20]</sup> that Nb as a solute has a strong tendency to segregate to the grain or interphase boundaries because of the large lattice misfit of Nb atoms in Fe. Although the equilibrium/nonequilibrium segregation of Nb has been studied,<sup>[21,22]</sup> there is still a lack of knowledge on segregation of Nb atom during welding thermal cycle. In the present study, the same Nb-bearing microalloyed steel that was used in our previous study<sup>[17]</sup> was employed. The distribution of Nb in the simulated coarse-grained heat-affected zone (CGHAZ) was studied by atom probe tomography (APT). It

H.H. WANG, Z. TONG, X.L. WAN, K.M. WU, and R. WEI are with The State Key Laboratory of Refractories and Metallurgy, Hubei Collaborative Innovation Center for Advanced Steels, International Research Institute for Steel Technology, Wuhan University of Science and Technology, Wuhan, China. Contact e-mail: wanghonghong@wust.edu.cn J. WANG, P.D. HODGSON, and I. TIMOKHINA are with the Institute for Frontier Materials, Deakin University, Geelong, Australia. Contact e-mail: ilana.timokhina@deakin.edu.au

Manuscript submitted April 12, 2018.

Article published online October 1, 2018

provides an understanding on the behaviors of Nb across prior austenite grain boundary (PAGB), ferrite/martensite-austenite interface (FMAI), and ferrite/ferrite interface (FFI) during the rapid cooling from high temperature. Further, it is suggested to be helpful in our understanding of the correlation between the resulting microstructure and good impact toughness for this investigated Nb-bearing steel.

## II. EXPERIMENTAL

The investigated steel was manufactured by hot rolling followed by rapid cooling. The chemical composition is given in Table I; Fe is balanced. The Gleeble 3800 simulator was used to simulate the welding thermal cycle by submerged arc welding with the heat input of around 35 kJ/cm to generate a CGHAZ. The samples were heated at 150 °C/s raising it to the temperature of 1320 °C, followed by cooling to 950 °C in 10 seconds. Then, the samples were quenched to room temperature to stabilize the grain boundary migration. In order to avoid formation of Nb carbides, the interrupted cooling temperature of 950 °C was chosen based on the calculated temperature of 900 °C for Nb carbide formation. Optical microscopy (OM) and transmission electron microscopy (TEM) were also performed to confirm the microstructure of CGHAZ. The OM samples were mechanically polished and etched with 4 pct Nital. The TEM samples were electropolished with 5 pct perchloric acid in methanol at voltage 25 V and – 35 °C temperature. The TEM observation was conducted through JEOL 2100F operated at 200 kV. Electron backscattered diffraction (EBSD) mapping was performed using a dual-beam scanning electron microscopy (FEI Quanta 3D) equipped with an EDAX-TSL EBSD system to characterize the microstructure of the samples. The EBSD samples were mechanically polished with diamond paste and finished with 50 nm colloidal silica. APT analysis was conducted to investigate the solute redistributions across the PAGB, FMAI, and FFI of CGHAZ. The PAGBs were identified as high-angle grain boundaries (~ 44 deg) in the EBSD map (Figure 1(a)). The APT samples of grain boundaries were prepared by site-specific *in-situ* lift-out (INLO) method<sup>[23]</sup> using focused ion beam (FIB) in FEI Quanta 3D. Representative EBSD map of a typical PAGB is shown in Figure 1(b), whereas the corresponding SEM image of the boundary area milled out using FIB is shown in Figure 1(c). The APT needles were sharpened to less than 100 nm in diameter with FIB at an operating voltage of 8 kV. As the bainitic laths are relatively thin, the INLO specimen not only contained PAGB, but also had FMAI and FFI positions near the PAGB. By fine controlling the milling depth, the PAGB, FMAI, and FFI were obtained within the tip of the APT needles. The APT experiments were carried out using Cameca LEAP 4000 HR, operated in voltage mode with a pulse rate of 200 kHz. Specimen temperature was controlled at 60 K, and the detection rate was maintained at 0.5 pct. Data reconstruction and quantitative

evaluation of APT datasets were performed using the software package, IVAS 3.6.12-14.<sup>[24]</sup>

## III. RESULTS

The initial microstructure after simulated welding thermal cycle consists of granular bainite (Figure 2(a)). Granular bainite is characterized by the absence of carbides and the presence of isolated regions of the retained austenite and martensite between crystals of bainitic ferrite (hereafter called ferrite), which have grain or plate morphology (Figure 2(b) and (c)). The volume fraction of retained austenite was measured using EBSD and was found to be less than 5 pct.

### A. Nb and C Segregation at PAGB

The atom maps and concentration profiles were used to study the chemical gradients across PAGB. The maps of C and Nb atom clearly showed the inhomogeneous redistribution of these atoms across the PAGB (Figure 3(a)). The strong C and Nb segregations formed at the PAGB, but there is no observation of Nb-carbides (Figure 3). The PAGB was positioned at the higher concentrations of C and Nb compared to the average concentration of these elements in the matrix (Figure 3(a)). Concentration profile of the Nb along the selected box (Figure 3(a)) showed that the Nb concentration increased from an average of 0.033 at. pct in the matrix up to 0.109 at. pct at the PAGB (Figure 3(b)). The enrichment factor, defined as an average concentration at grain boundary divided by the average bulk concentration, was used to measure the amount of Nb segregation.<sup>[23]</sup> The enrichment factor of Nb at PAGB was measured to be 3.12. The C concentration profile along the selected box showed the build-up of a C spike from an average of 0.10 in the matrix to 1.80 at. pct at the PAGB (Figure 3(c)). The enrichment factor of C was 14.94 at the PAGB.

### B. Nb and C Segregations at FMAI

The distribution of the solutes across FMAI was also studied using APT. As shown in the representative carbon atom map (Figure 4(a)), there are two distinct regions with different carbon contents. The low-carbon region is corresponding to the bainitic ferrite phase, whereas the high-carbon region is the martensite-austenite constituent. It should be noted here that it was not possible to make a distinction between the martensite and the retained austenite from the APT carbon atom maps since all the retained austenite regions in the microstructure were transformed to martensite during the cooling to the APT analysis temperature of 60 K. Compositional analyses of several C atom maps allowed an estimation of the average C content of bainitic ferrite of  $0.25 \pm 0.08$  at. pct and martensite of  $3.75 \pm 0.03$  at. pct. The position of the interface between ferrite and martensite was defined based on the concentration of main elements such as C and Mn in ferrite and martensite. The interface was positioned at the midpoint

Table I. Composition of the Investigated Steel

	C	Si	Mn	Cr	Mo	Nb	V	Ti	B	Al	P	S
wt pct	0.05	0.17	0.78	0.50	0.20	0.09	0.03	0.015	0.0002	0.033	0.01	0.001
at. pct	0.24	0.34	0.80	0.54	0.12	0.06	0.03	0.02	0.001	0.07	0.02	0.002

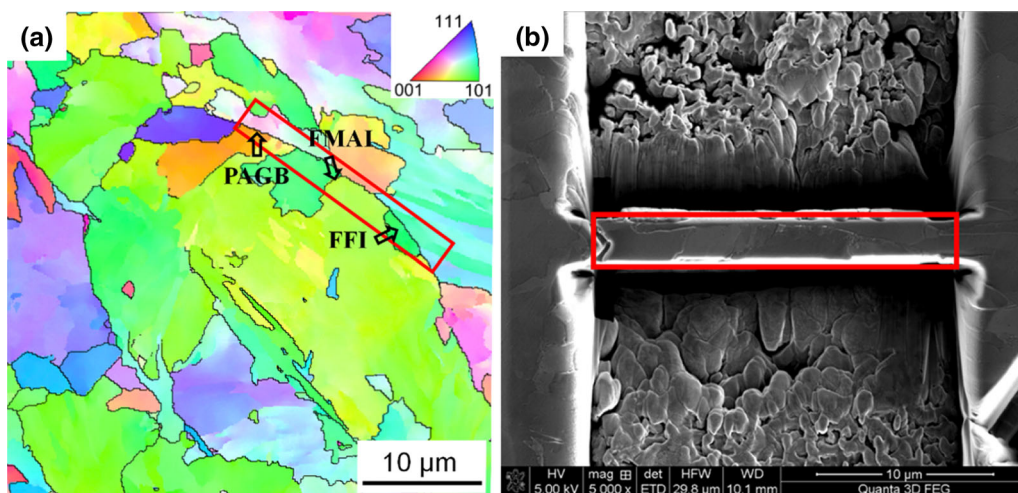


Fig. 1—(a) IPF and EBSD maps of the CGHAZ microstructure and the area with PAGB selected for *in-situ* lift-out (INLO) APT samples; (b) corresponding SEM images of areas for INLO samples from PAGB shown in (a).

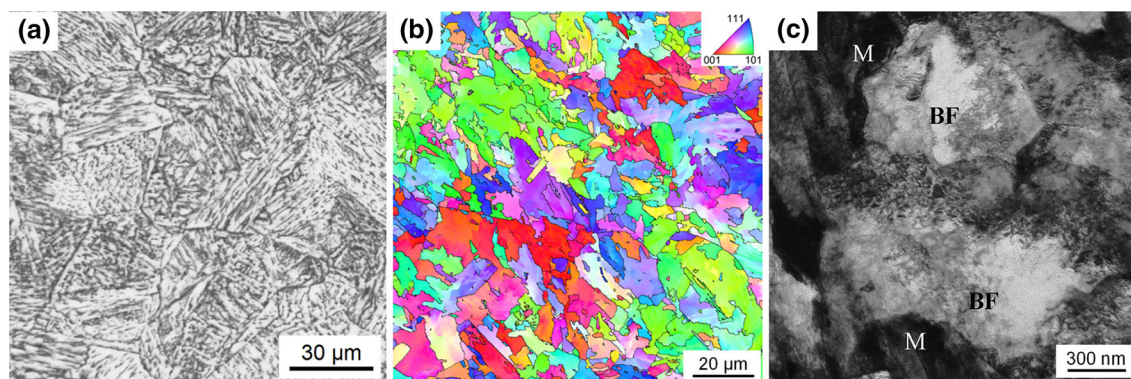


Fig. 2—(a) Optical, (b) EBSD, and (c) TEM micrographs of simulated CGHAZ. M is martensite and BF is bainitic ferrite.

of the concentration difference in C between martensite and ferrite (Figure 4(c)).

The average concentration of Nb in martensite was higher ( $\sim 0.12 \pm 0.02$  at. pct) than that in ferrite ( $\sim 0.06 \pm 0.02$  at. pct). The Nb concentration spike of 0.21 at. pct at the ferrite/martensite interface was observed (Figure 4(b)). Given that the Nb concentration was 0.06 at. pct in the ferrite matrix, the enrichment factor of Nb was calculated to be 3.50 at the FMAI. This indicates that the Nb segregation is stronger at FMAI than at PAGB.

### C. Nb and C Segregations at FFI

The solute redistribution across FFI was also investigated using APT (Figure 5). The site-specific

APT samples (Figure 5(a)) were taken from a ferrite grain having low misorientation-angle subgrains, as shown in the white dashed area in Figure 5(b). The orientation relationship between the neighboring ferrite grains of the studied FFI (grains A and B, Figure 5(a)) cannot be directly identified from EBSD maps, as the interface and grain B (Figure 5(a)) were located under the sample surface. However, it is possible to determine the orientation of ferrite grain A (black star) and its neighboring grains (red dots) from EBSD map and [001] pole figure (Figure 5(b)). It appeared that all subgrains shared the same Bain variant, and the misorientation angles are  $< 10$  deg. It is highly likely that the FFI in the APT sample between grains A and B also has a low misorientation angle.



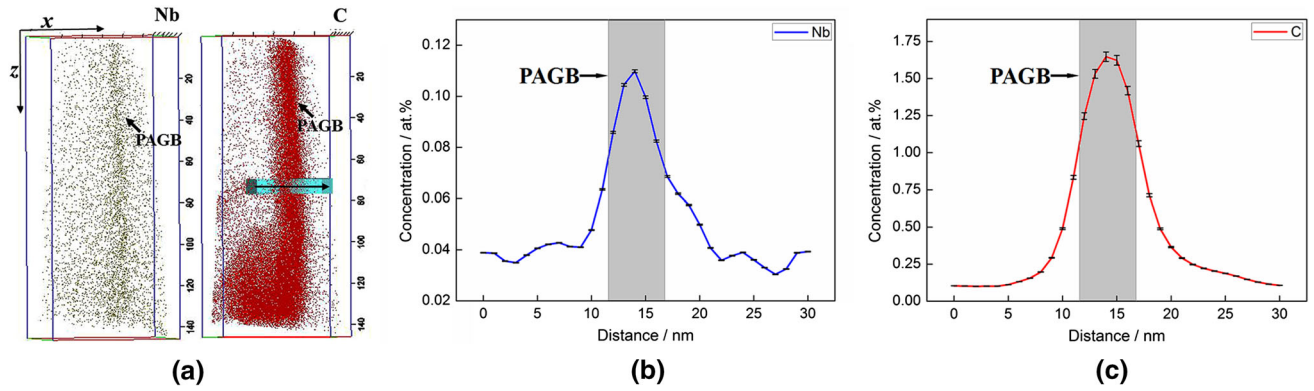


Fig. 3—(a) Representative Nb and C atom maps of (b) Nb and (c) C-compositional profiles across the PAGB interface along the direction identified by arrow within the selected box shown in (a). Gray zones in (b, c) represent the positions of grain boundary.

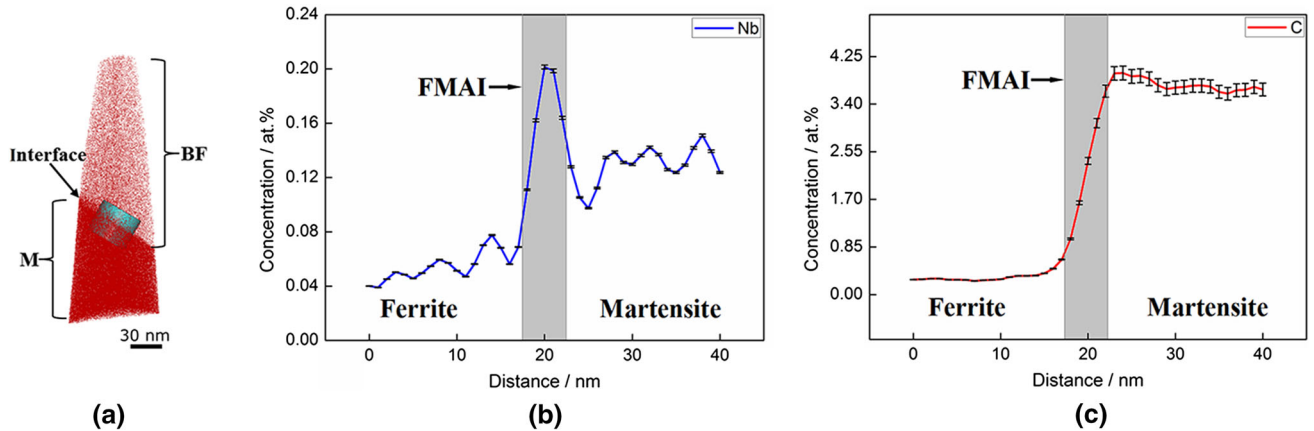


Fig. 4—(a) Representative carbon atom maps of Martensite (M) and Bainitic ferrite (BF), (b) Nb and (c) C-compositional profile across the interface shown in (a). Gray zones in (b, c) represent the positions of the interface.

APT carbon map confirmed slight segregation of C at the FFI between bainitic ferrite grains A and B (Figure 5(a)). Interestingly, 1-D concentration profile across FFI (Figure 5(a)) revealed two Nb ( $\sim 0.045$  at. pct) and two carbon peaks of  $\sim 0.2$  and  $0.1$  at. pct. However, the second peaks of Nb and C (Figures 5(c) and (d)) were from another FFI, which is located behind the primary FFI, and is not considered here for discussion. We assumed the concentration profile was measured near a triple junction point.

As the average concentrations of Nb and C in the nearby matrix (area without visible solutes segregations) were  $\sim 0.025$  at. pct Nb and  $0.05$  at. pct C, the enrichment factors of Nb and C at FFI were calculated to be  $1.8$  and  $4.0$ , respectively. This indicates that the segregations of Nb and C at the FFI are much weaker than those at the PAGB and FMAI, which could be due to the low angle of grain boundary misorientation observed for these ferrite grains. The ferrite matrix has become depleted with Nb compared to the bulk steel composition ( $0.06$  at. pct) due to Nb segregation on PAGB and FMAI, which consumes considerable amount of Nb atoms.

## IV. DISCUSSION

### A. Solute Distribution of Nb During Welding Thermal Cycle

Niobium showed pronounced segregations at PAGB, FMAI, and FFI during the welding thermal cycle. This is because the radius ratio of  $r_{\text{Fe}}/r_{(\text{Fe-Nb})}$  is as high as  $6.6:1$ .<sup>[19]</sup> The large lattice misfit of Nb atoms in Fe leads to lower solubility and segregation of Nb in Fe.<sup>[19]</sup> Segregation of Nb can be of equilibrium and/or nonequilibrium depending on the heat-treatment condition.<sup>[21,22]</sup> It appeared that the simulated welding thermal cycle with fast cooling from high temperature can stimulate the nonequilibrium segregation as the dominant mechanism. The significance of nonequilibrium segregation of a solute strongly depends on its binding energy with vacancies. The binding energies  $E_b$  between a vacancy and Nb are calculated using the equation<sup>[25]</sup>:

$$E_b = 8\pi\mu r_0^3 \varepsilon^2, \quad [1]$$

where  $\mu$  is the shear modulus of matrix,  $r_0$  is the radius of Fe, and  $\varepsilon$  is the misfit of Nb in Fe,  $\varepsilon = (r_{\text{Nb}} - r_{\text{Fe}})/$

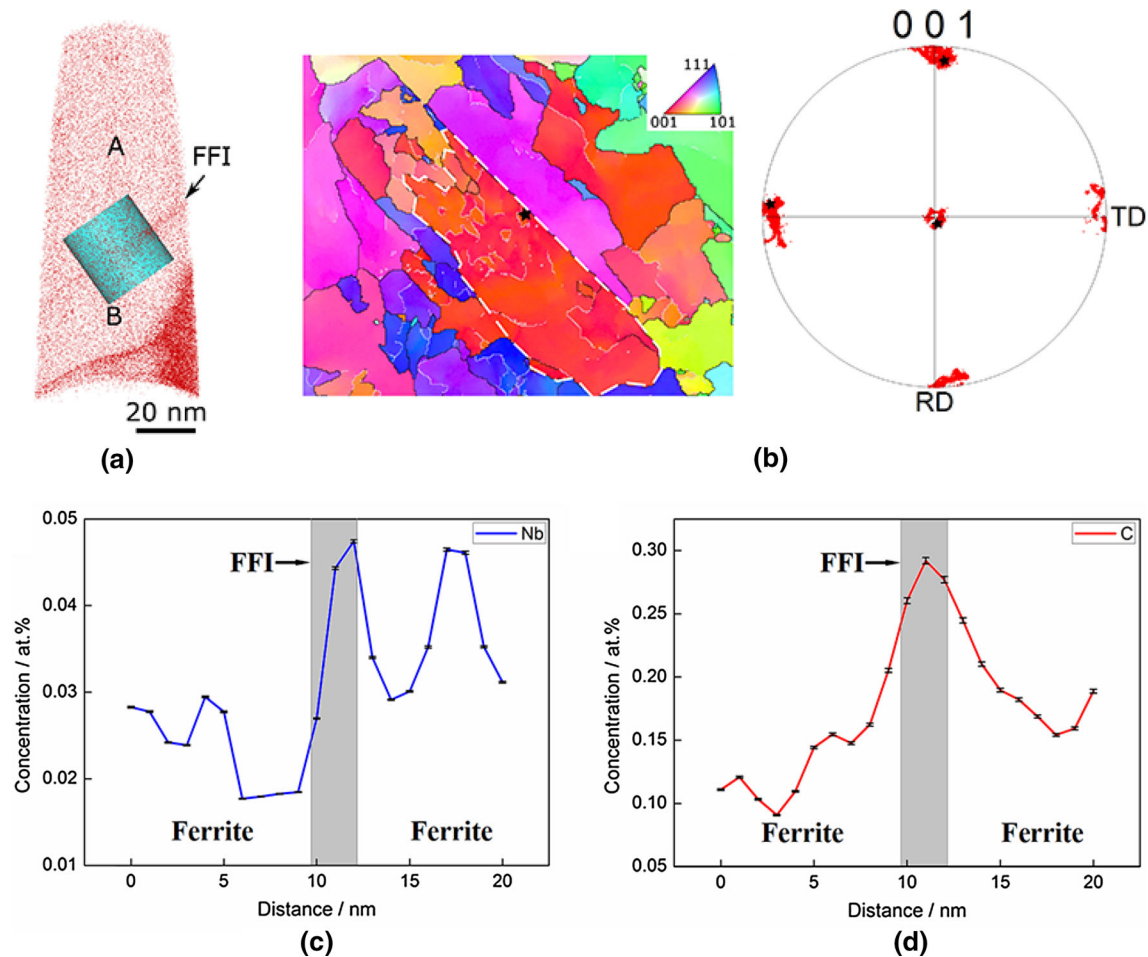


Fig. 5—(a) Representative carbon atom map showing segregation of C at FFI. (b) EBSD map and [001] pole figure showing the orientation of the ferrite grain A in the APT sample (black star) and its neighboring grains (red dots). (c) Nb and (d) C-concentration profiles across the FFI along the selected box shown in (a). Gray zones in (c, d) represent the position of interface (Color figure online).

$r_{Fe}$ . In the present study,  $E_b$  for Nb is 0.45 eV, which is in the range of  $\sim 0.15$  to 0.60 eV for the occurrence of nonequilibrium grain boundary segregation, as suggested by Xu.<sup>[26]</sup> Hence, the strong Nb segregations at PAGB, FMAI, and FFI are well expected during the welding thermal cycle. In addition, due to the strong segregation at grain boundaries and interfaces, the concentration of Nb in matrix (0.03 at. pct) was lower than the nominal concentration (0.06 at. pct).

It was suggested that Nb segregation at PAGB occurred during cooling process, including both stages: lowering of high temperature from 1320 °C to 950 °C and quenching from 950 °C to room temperature, while Nb segregations at FMAI and FFI occurred during quenching, especially transformation from austenite to bainite. During quenching at lower temperature below 950 °C, Nb is difficult to diffuse. Thus, the formation of Nb-vacancy complex and diffusion into interfaces may be the dominant mechanism. While, at higher temperature from 1320 °C to 950 °C,

Nb can easily diffuse to grain boundaries driven by Gibbs free energy. Its segregation mechanism need to be further investigated.

More importantly, the Nb had different enrichment factors at PAGB, FMAI, and FFI. This is attributed to the different misorientation angles at these boundaries and interfaces. The boundary with a large misorientation angle is prone to attract solute atoms due to the high binding energy.<sup>[27]</sup> Because the PAGB and FMAI are high-angle grain boundaries and FFI is small-angle grain boundary, Nb has a higher segregation tendency at PAGB and FMAI than at FFI.

There was no NbC particle detected by APT, as shown in Figure 2. This is because of the fast cooling rate after 950 °C. However, the ratio of carbon to niobium was  $\sim 10$  at PAGB, which was higher than the carbon-to-niobium ratio ( $\sim 2.80$ ) during the early stage of NbC precipitation.<sup>[28]</sup> Similarly, the ratio of carbon to niobium was  $\sim 6$  at FFI, which was also higher than  $\sim 2.80$ . Thus, it is suggested that if the cooling rate is

slow enough, NbC could precipitate at PAGB and FFI during continuous cooling.

### B. Calculation of Segregation Energy

Segregation of solute elements at grain boundary leads to change in grain boundary energy, which is an important parameter that determines solute drag behavior. According to the Langmuir–McLean isotherm,<sup>[29]</sup> the segregation energy, which is defined as the change in Gibbs free energy caused by solute segregation, can be estimated as

$$\Delta G_b = -RT \left[ \frac{1 - X_M}{X_M} \cdot \frac{\theta_B}{1 - \theta_B} \right], \quad [2]$$

where  $X_M$  is the fraction of the solute element in the matrix, and  $\theta_B$  is the solute coverage ratio on the grain boundary. The value of  $\theta_B$  can be calculated from

$$\theta_B = \frac{\Gamma^s}{\Gamma^0}, \quad [3]$$

where  $\Gamma^0$  is a boundary excess of solute constituting a monolayer of unit area, ( $\Gamma^0$  for  $\alpha$ -Fe  $\sim 1.60 \times 10^{19}$  atoms/m<sup>2</sup>), and  $\Gamma^s$  is the interfacial excess of solute element. According to the method described in Reference 30,  $\Gamma^s$  can be obtained as

$$\Gamma^s = \frac{N_{\text{excess}}}{A}, \quad [4]$$

wherein  $N_{\text{excess}}$  is the excess number of solute atoms detected at the grain boundaries and  $A$  is the area of analyzed cross section. In the present study,  $N_{\text{excess}}$  of Nb is measured to be 192.10 and  $A$  is 1802 nm<sup>2</sup> (Figure 6). Thus, the corresponding value for  $\Gamma^{\text{Nb}}$  determined by APT is  $0.27 \times 10^{19}$  atoms/m<sup>2</sup> and  $\theta_B$  is calculated using Eq. [3] to be 0.17.

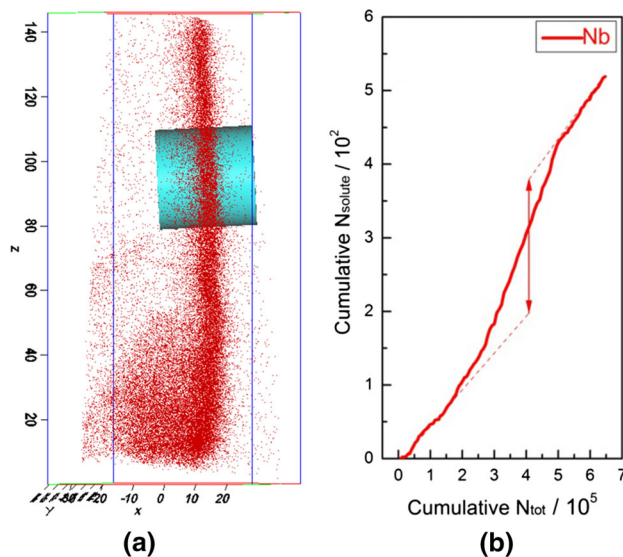


Fig. 6—(a) Carbon atom map and selected box used for calculation of excess number of Nb solute atoms segregated at PAGB (b).

Assuming that there is only one type of boundary site and no site-to-site interactions, the segregation energy of Nb at the PAGB was calculated to be 22.91 kJ/mol at 950 °C. It should be noted that due to the strong interaction of niobium and carbon, co-segregation of niobium and carbon occurs. Therefore, the segregation energy of 22.91 kJ/mol should be an overestimated value if it is attributed to Nb only. This segregation of Nb can reduce the ferrite growth rate drastically during transformation on cooling. Meanwhile, the diffusivity of Nb in the grain boundary decreases with the increasing Nb content at the grain boundaries.<sup>[31]</sup> Thus, the solute drag effect of Nb,<sup>[32–34]</sup> combined with other alloying element on continuous cooling transformation, is likely to be observed.

The segregation of niobium to FMAI promotes a diffusion of carbon into FMAI, because of strong affinity between niobium and carbon. This interaction hinders the diffusion of carbon from ferrite.<sup>[17]</sup> The segregation of Nb at the FMAI retards the migration of the FMAI, due to the solute drag effect. On the other hand, higher content of carbon of 3.5 to 4.0 at. pct within the retained austenite (RA) is expected to significantly decrease the martensite start temperature ( $M_s$ ) and thus enhance the stability of RA. Notably, Nb content remained high at  $\sim 0.15$  at. pct within the M-A constituent. Niobium is a ferrite stabilizer. However, addition of up to 0.10 to 0.20 wt pct niobium lowers the  $A_3$  temperature, when Nb acts as an austenite stabilizer.<sup>[35]</sup> Therefore, the chemical potential of solute Nb atoms in M-A constituent is higher than that in ferrite.<sup>[36]</sup> Although no effect of Nb is present in  $M_s$  Equation,<sup>[37]</sup> the  $\sim 0.15$  at. pct Nb will play positive role in stabilizing the RA during the cooling process. The enhanced stability of retained austenite is beneficial to impact toughness. The segregations of Nb and C at FFI reduce the interface energy. Thus, the migration of interface is inhibited, and the ferrite lath width is expected to be refined. The fined ferrite matrix is also beneficial to impact toughness.

The individual extents of niobium segregation at PAGB, FMAI, and FFI were different. Thus, Nb and other elements were lean in the matrix. As shown in Figures 2 through 4, Nb content was  $\sim 0.02$  to 0.04 at. pct, and C content was  $\sim 0.1$  to 0.3 at. pct in matrix. The lean austenite may have decreased stability, and its decomposition temperature may be increased.<sup>[38]</sup>

## V. CONCLUSIONS

The segregation behaviors of niobium and carbon at prior austenite grain boundary, ferrite-M-A constituent interface, and ferrite-ferrite interface during simulated welding thermal cycle from high temperature of 1320 °C in niobium-bearing microalloyed steel were studied using atom probe tomography. APT analysis provided specific information on the chemical composition and distribution of alloying elements.

- (1) During welding thermal cycle, Nb segregated strongly at PAGB and FMAI. The enrichment



factor of Nb was as high as 3.12 and 3.50 at the PAGB and FMAI, respectively. In contrast, minimal Nb segregation occurred at the FFI, with an enrichment factor of only 1.80.

- (2) The binding energy of Nb and vacancy is calculated to be 0.45 eV, indicating that Nb segregation during welding thermal cycle is probably attributable to the nonequilibrium segregation.
- (3) The interfacial excess of Nb solute element  $\Gamma^{\text{Nb}}$  at PAGB determined by APT is  $0.27 \times 10^{19}$  atoms/m<sup>2</sup>. The Nb segregation can decrease the Gibbs energy by 22.91 kJ/mol at the PAGB. This can explain the fine bainitic structure in the Nb-bearing microalloyed steel after welding, because the strong Nb segregation at PAGB can effectively prevent the growth of austenite grains at high temperature, whereas those at FMAI can restrain the growth of bainitic ferrite during cooling.

### ACKNOWLEDGMENTS

The authors gratefully acknowledge the financial supports received from National Natural Science Foundation of China (No. 51601135), Hubei Province, for 1000 talent program and the Australia research council *via* a discovery project. The permission for the use of the equipment—FEI Quanta 3D SEM and Cameca LEAP 4000 HR—at the Deakin University's Advanced Characterization Facility is also gratefully acknowledged.

### REFERENCES

1. P. Kirkwood: *The Chinese Society for Metals (CSM) and Chinese Academy of Engineering (CAE), Hangzhou, China*, 2015, pp. 439–45.
2. E. El-Kashif, and T. Koseki: *Chapter 4 Effect of Niobium on HAZ Toughness of HSLA Steels. Alloy Steel—Properties and Use*, 2011, INTECH.
3. Y.Q. Zhang, H.Q. Zhang, J.F. Li, and W.M. Liu: *J. Iron. Steel Res. Int.*, 2009, vol. 16, pp. 73–80.
4. N.E. Hannerz: *Weld. J. Res. Suppl.*, 1975, vol. 5, pp. 162–68.
5. K. Hulka, and F. Heisterkamp: *ASM*, 1984, pp. 915–24.
6. R.J. Hattingh and G. Pienaar: *Int. J. Pres. Ves. Pip.*, 1998, vol. 75, pp. 661–77.
7. S. Shanmugam, R.D.K. Misra, T. Mannering, D. Panda, and S.G. Jansto: *Mater. Sci. Eng., A*, 2006, vol. 437, pp. 436–45.
8. A.B. Rothwell: *Heat-Affected Zone Toughness of Welded Joints in Microalloyed Steels, Part I. IIW Document*. 1979, vol. IX-1147–80.
9. R.E. Dolby: *Res. Bull.*, 1977, vol. 7, pp. 298–313.
10. B. Hutchinson, J. Komenda, G.S. Rohrer, and H. Beladi: *Acta Mater.*, 2015, vol. 97, pp. 380–91.
11. Y.Q. Zhang, H.Q. Zhang, W.M. Liu, and H. Hou: *Mater. Sci. Eng., A*, 2009, vol. 499, pp. 182–86.
12. P.R. Kirkwood: *The Weldability of Modern Niobium Microalloyed Structural Steels* Singapore, 2012, vol. 12, pp. 5–7.
13. Y. Li, D.N. Crowther, M.J.W. Green, P.S. Mitchell, and T.N. Baker: *ISIJ Int.*, 2001, vol. 41, pp. 46–55.
14. C. Fossaert, G. Rees, T. Maurickx, and H.K.D.H. Bhadeshia: *Metall. Mater. Trans. A*, 1995, vol. 26A, pp. 21–30.
15. T. Furuhashi, T. Yamaguchi, G. Miyamoto, and T. Maki: *Mater. Sci. Technol.*, 2010, vol. 26, pp. 392–97.
16. F. Barbaro, Z.X. Zhu, L. Kuzmilova, H.J. Li, and H. Jian: *TMS 2015, Hangzhou, International Conference in HSLA Steels 2015, Microalloying 2015 & Offshore Engineering Steels*, 2015, pp. 453–57.
17. H.H. Wang, Z.P. Qin, X.L. Wan, R. Wei, K.M. Wu, and R.D.K. Misra: *Met. Mater. Int.*, 2017, 23.
18. I. Timokhina, P.D. Hodgson, and E. Pereloma: *Mater. Trans. A.*, 2004, vol. 35, pp. 2331–41.
19. D. McLean: *Grain Boundaries in Metals*, Clarendon Press, Oxford, 1957, p. 124.
20. H. Jin, I. Elfimov, and M. Militzer: *J. Appl. Phys.*, 2014, vol. 15, pp. 093506–1–8.
21. N. Maruyama, G.D.W. Smith, and A. Cerezo: *Mater. Sci. Eng., A*, 2003, vol. 353, pp. 126–32.
22. J.F. Peter, R.K. Chris, G.W. Jim, R.C. Kristin, P.R. Simon, and M.C. Julie: *Acta Mater.*, 2012, vol. 60, pp. 5049–55.
23. L. Karlsson: *Acta Metall.*, 1988, vol. 36, pp. 25–34.
24. M.K. Miller and R.G. Forbes: *Atom-Probe Tomography: The Local Electro Atom Probe*, Springer, New York, 2014.
25. A.H. Cottrell: *An Introduction to Metallurgy*, Edward Arnold, London, 1967.
26. T.D. Xu: *Scripta Mater.*, 1997, vol. 37, pp. 1643–50.
27. L. Karlsson, H. Norden, and H. Odellius: *Acta Metall.*, 1988, vol. 36, pp. 1–12.
28. F. Danoix, E. Bémont, P. Maugis, and D. Blavette: *Adv. Eng. Mater.*, 2006, vol. 8, pp. 1202–05.
29. D. McLean: *Grain Boundaries in Metals*, Clarendon Press, Oxford, 1957, p. 116.
30. B.W. Krakauer and D.N. Seidman: *Phys. Rev. B.*, 1993, vol. 48, pp. 6724–27.
31. M. Suehiro, Z.-K. Liu, and J. Ågren: *Acta Mater.*, 1996, vol. 44, pp. 4241–51.
32. C. Sinclair, C. Hutchinson, and Y. Bréchet: *Metall. Mater. Trans. A*, 2007, vol. 38A, pp. 821–30.
33. T. Gladman: *The Physical Metallurgy of Microalloyed Steels Institute of Materials*, Institute of Materials, Minerals & Mining (IOM3), London, 1997.
34. C.R. Hutchinson, H.S. Zurob, and Y. Bréchet: *Metall. Mater. Trans.*, 2006, vol. 37, pp. 1711–20.
35. A.J. DeArdo: Niobium in modern steels *Int. Mater. Rev.*, 2003, vol. 48, pp. 371–402.
36. L. Wang, S. Parker, A. Rose, G. West, and R. Thomson: *Metall. Mater. Trans. A*, 2016, vol. 47A, pp. 3387–96.
37. C. Capdevila, F.G. Caballero, and C. Garcia de Andrés: *ISIJ Int.*, 2002, vol. 42, pp. 894–902.
38. H.K.D.H. Bhadeshia and R.W.K. Honeycombe: *Steels: Microstructure and Properties*, 3rd ed., University of Cambridge, Cambridge, 2006, p. 117.